A. Tzamtzis et alii, Frattura ed Integrità Strutturale, 35 (2016) 396-404; DOI: 10.3221/IGF-ESIS.35.45

Focussed on Crack Paths

Fatigue crack growth prediction in 2xxx AA with friction stir weld HAZ properties

A. Tzamtzis, A. T. Kermanidis
Laboratory of Mechanics and Strength of Materials, Department of Mechanical Engineering, University of Thessaly, Leoforos Athinon, Pedion Areos 38334, Volos, Greece
atzam@uth.gr, akermanidis@mie.uth.gr

ABSTRACT. An analytical model is developed to predict fatigue crack propagation rate under mode I loading in 2024 aluminum alloy with FSW HAZ material characteristics. Simulation of the HAZ local properties in parent 2024 AA was performed with overaging using specific heat treatment conditions. The model considers local cyclic hardening behavior in the HAZ to analyze crack growth. For the evaluation of the model, the analytical results have been compared with experimental fatigue crack growth on overaged 2024 alloy simulating material behavior at different positions within the HAZ. The analytical results showed that cyclic hardening at the crack tip can be used successfully with the model to predict FCG in a material at overaged condition associated with a location in the FSW HAZ.

KEYWORDS. Fatigue Crack Growth Analysis; Aluminum Alloy; Friction Stir Weld; Heat Affected Zone; Cyclic Hardening.

INTRODUCTION

Fatigue crack growth rate (FCG) is influenced by several complex interactive processes that involve microstructural and mechanical load variables. Models used for analysis of crack growth rate under constant amplitude stress include a hierarchy of major simplifications, with most important being the application of the linear elastic fracture mechanics (LEFM) concept and are mainly empirical or semi-empirical because they rely on fitting experimental material crack growth data [e.g 1]. Early models based on damage accumulation at the crack tip have a more physical background but use parameters that are difficult to determine experimentally [2-4]. In more recent modeling attempts [5-8], authors have used the cyclic material behavior at the crack tip to derive analytical expressions for the fatigue crack growth rate. Again, most of the models include geometrical (crack tip blunting radius) or material parameters (stress intensity factor threshold), which cannot be derived from simple tests. In [9], a fatigue crack growth model is developed, which considers a strip plastic zone with material hardening at the tip of a crack, under low cycle fatigue conditions, which uses few experimental parameters for fatigue crack growth analysis. In the above approaches a homogeneous material is considered and properties used for prediction are average material properties of the material volume examined.
If a crack grows within a material zone with varying microstructure the analysis is more complicated and local material behavior needs to be implemented. In the early work by Reifsnider et al. [10] it was found that the existence of a strength gradient at the tip of the crack, depending on its slope, may accelerate or retard crack growth. This is relevant in the case of the heat affected zone (HAZ) in a weld region, where the aged material consists of a modified microstructure with local

material properties in the HAZ area. In the HAZ fatigue crack growth rate is influenced by the inhomogeneous overaged microstructure [11-13]. In [14] it was shown that overaging of 2024 material has significant impact on the fatigue crack growth behavior of the alloy. A relevant mechanism of 2024 alloy influenced by overaging [14], which is associated with the material's fatigue crack growth rate is cyclic strain hardening at the crack tip. In studies [15-17], cyclic strain hardening has been linked analytically and experimentally to the closure levels of the advancing crack and hence the rate of its propagation. This dependency has been exploited in the fatigue crack growth analysis, to include the effect of local material properties on FCG with the variation in cyclic strain hardening behavior at different locations in the HAZ. The model assumes LCF conditions at the crack tip and considers incremental crack growth under fatigue loading. The results obtained analytically are compared with experimental fatigue crack growth data on overaged 2024 aluminum alloy simulating different local properties and microstructure within the HAZ.

CRITICAL ENERGY DISSIPATION FOR CRACK GROWTH

In the proposed model crack growth occurs incrementally after a critical number of cycles ΔN. The crack growth increment Δr is equal to a material element with width Δr at the crack plane (Fig. 1). Based on these assumptions, a crack propagation rate can be calculated from equation:

$$\frac{da}{dN}=\frac{\Delta r}{\Delta \mathrm{N}} \tag{1}$$

It is assumed that the material element at the crack tip is subjected to low cycle fatigue conditions [5-9] with an average constant plastic strain range $\Delta\varepsilon_{pm}$. Under cyclic straining material failure occurs when in a stabilized hysteresis loop a critical amount of energy W_f is accumulated in the material after a finite number of loading cycles N_f. By assuming that the energy per cycle ΔW is nearly constant throughout the fatigue test, the total plastic strain energy until fracture may be approximated by [18]:

$$W_f=\Delta W\cdot N_f=2\sigma_A\cdot\Delta\varepsilon_p\left(\frac{1-n'}{1+n'}\right)N_f \tag{2}$$

with σ_A the stress amplitude and n' the cyclic strain hardening exponent. The critical amount of energy W_f for failure of the material volume is estimated from the strain energy density [SED] theory [19-20]. In the SED criterion the critical strain energy density function dW/dV is associated with the critical distance r_c from the crack tip for onset of crack initiation and the critical strain energy density factor S_c in the form:

$$\left(\frac{dW}{dV}\right)_c=\frac{S_c}{r_c} \tag{3}$$

For plane stress the strain energy density factor becomes:

$$S_c=\frac{(1-\nu)K_{cr}^2}{2\pi \mathrm{E}} \tag{4}$$

Assuming that the energy for fracture can be approximated by the critical strain energy per unit volume $(dW/dV)_c$ from the SED criterion in Eq. (3), W_f in Eq. (2) can be derived with the use of Eq. (3) and the critical number of cycles N_f for a crack increment $\Delta r = r_c$ can be obtained from (2) by:

$$N_f=\frac{(1-\nu)\mathrm{K}_{cr}^2(1+n')}{4\pi \mathrm{E} r_c\sigma_{\mathrm{A}}\Delta\varepsilon_p(1-n')} \tag{5}$$

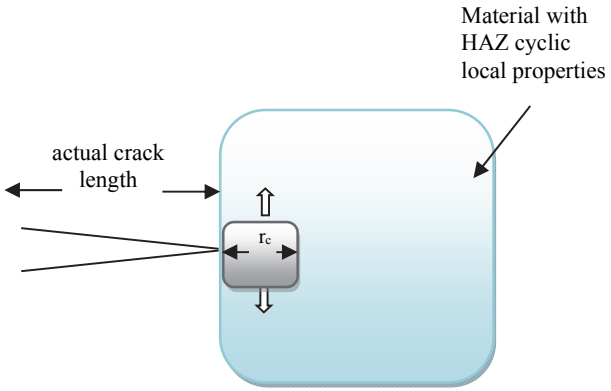

Figure 1: Incremental crack growth in HAZ.

By calculating in Eq. (5) for mode I loading the stress amplitude σ_A at the position of fracture r_c for an isotropic linear elastic material and by and using the Coffin-Manson relationship [21-22] to derive $\Delta\varepsilon_{p,}$ the crack growth equation can be derived:

$$\frac{d\alpha}{dN}=r_c^{\frac{2c+3}{2c+2}}\left[\frac{4\sqrt{\pi}\mathrm{E}2^{\left(c+\frac{1}{2}\right)}\left(1-n'\right)\varepsilon_f^{'}}{\left(1-v\right)\mathrm{K}_{cr}^{2}\left(1+n'\right)}\right]^{1/c+1}\left(\Delta\mathrm{K}\right)^{1/c+1} \tag{6}$$

Eq. (7) can be written in the following simplified form:

$$\frac{d\alpha}{dN}=A^{k}B^{m}\left(\Delta\mathrm{K}\right)^{m} \tag{7}$$

where parameter m is related to the Coffin-Manson parameter m as m=1/c+1
and

$$A=r_c \tag{8}$$

$$k=\frac{2c+3}{2c+2} \tag{9}$$

$$B=\left[\frac{4\sqrt{\pi}\mathrm{E}2^{\left(c+\frac{1}{2}\right)}\left(1-n'\right)\varepsilon_f^{'}}{\left(1-v\right)\mathrm{K}_{cr}^{2}\left(1+n'\right)}\right] \tag{10}$$

Parameters n', K_{cr}, c, ε_f', E can be determined experimentally. Crack growth rate in Eq. (7) is dependent on parameter B, which includes material properties and therefore provides a physical background in the crack growth analysis. The only fitting parameter I Eq. (7) is length r_c, which is also an undefined parameter in the SED theory.

EXPERIMENTAL SIMULATION OF HAZ LOCAL PROPERTIES

Microstructural Characteristics

Simulation of HAZ material properties was achieved by implementing a heat treatment procedure on 2024 material described in [14] using different overaging conditions. The procedure selected helps to produce materials based on the 2024 alloy with similar microstructural characteristics and local properties with selected positions in the HAZ, without the weld residual stresses. The overaged materials exhibit similar local properties and microstructural characteristics with 3 locations in the HAZ: (a) close to the base material, (b) at the mid-point of HAZ hardness gradient and (c) close to the weld nugget (HAZ/TMAZ interface), and are named A200, A250 and A300 respectively, based on the temperature of heat treatment used for 15 hours aging. The microstructural characteristics between the HAZ material (close to the base metal, 12 mm away from the weld center) and A200 are given in Fig. 2. They are comparable and consist of same size coarsened second-phase particles, the Al_2Cu (θ' phase) and the Al_2CuMg (S' phase). In both materials similar hardness values are obtained as shown in the hardness profile of the 2024 aluminum alloy FSW, in Fig. 3. In the same Figure, the hardness values of materials A250 and A300 are shown and are placed on the respective locations in the HAZ with similar hardness values.

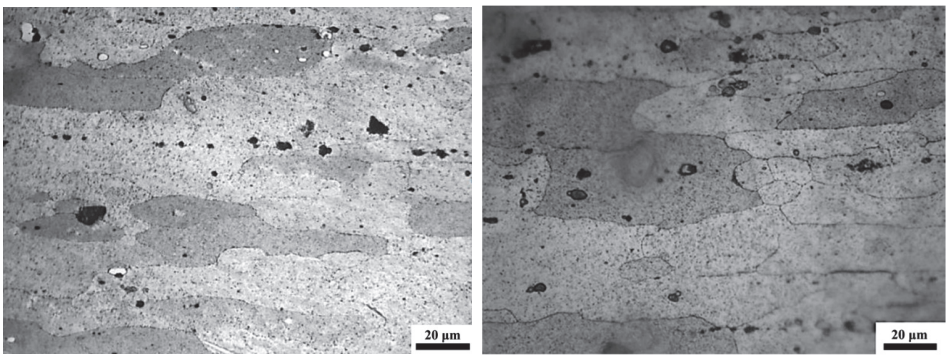

(a) (b)

Figure 2: Microstructures of (a) HAZ at a distance 12mm from the weld centerline, (b) A200 material.

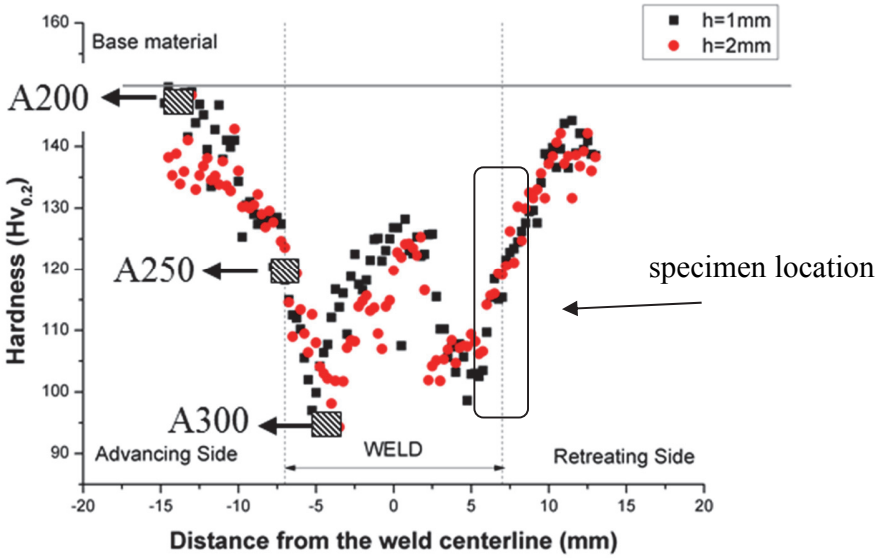

Figure 3: Microhardness variation in 2024 FSW determined at two different layers in the cross section of the FSW joint (1 and 2 mm depth from specimen surface). Local hardness values of A200, A250 and A300 materials are shown at the locations in the HAZ with similar microhardness values. The specimen location designates where the sample has been extracted to obtain local tensile properties in the HAZ.

Tensile behavior

The tensile stress-strain behavior of a subsize specimen (ASTM E8M-01) extracted from the location shown in Fig. 3 and the A250 material are compared up to a tensile strain of 5% in Fig. 4. The hardness of A250 material, is similar to the hardness obtained at the mid-point of the specimen gauge length in Fig. 3. Despite the small difference in strength values, the strain hardening behavior in the two cases is very close and the determined strain hardening exponent values are 0.150 and 0.161 for the HAZ and A250 materials respectively.

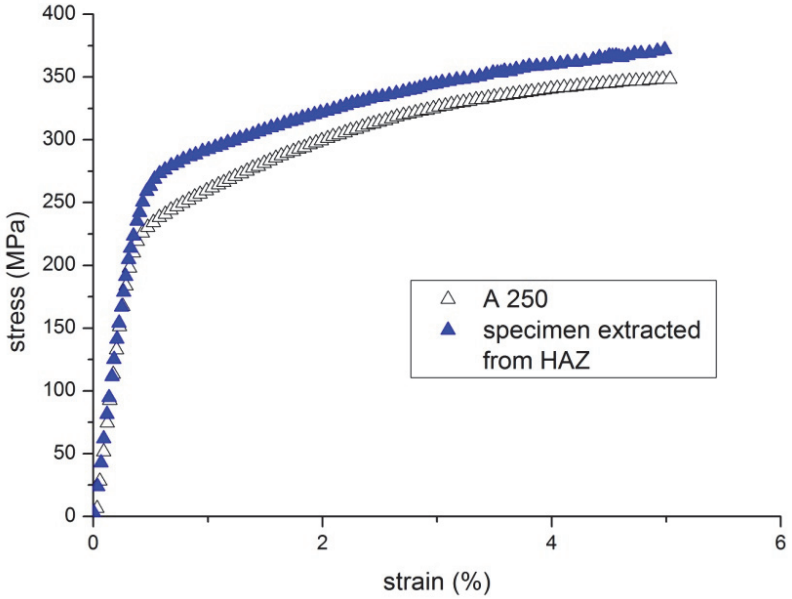

Figure 4: Stress strain curves for materials A 250 and HAZ at the mid-length of hardness gradient.

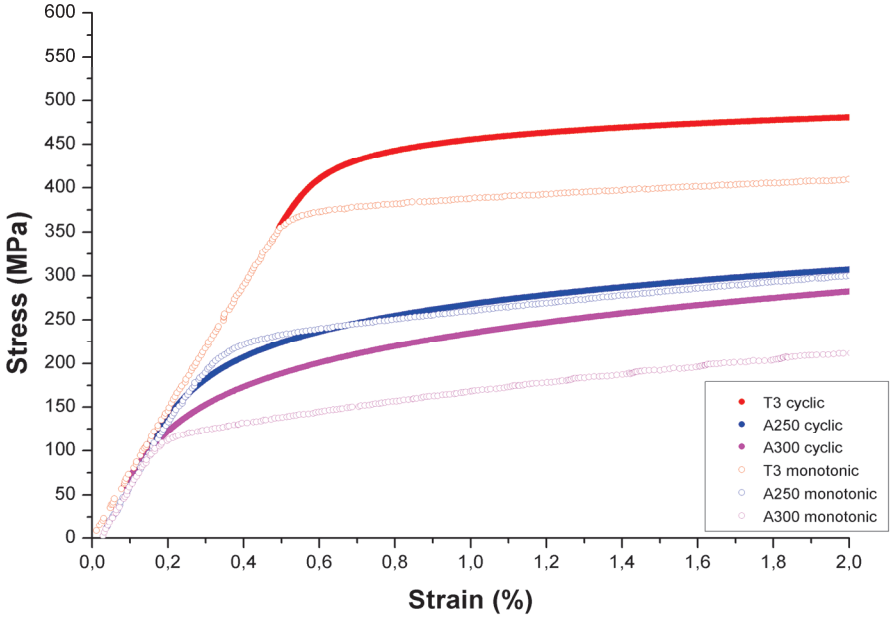

Figure 5: Monotonic & cyclic stress- strain curves of T3, A250 and A300 materials.

Cyclic hardening

The cyclic tests performed in [14] and reproduced in Fig. 5 show that cyclic strain hardening occurs in the overaged materials A250 and A300. Cyclic strain hardening after overaging is more pronounced compared to the base metal (T3) as obtained from the cyclic strain hardening exponent n' values in Tab. 1. Parameter n' increases with increasing overaging temperature (A300 material). This is associated with the HAZ location close to the weld center. The dependency of increasing cyclic strain hardening with increasing crack closure was investigated in [14]. Here, this dependency is used to analyze the crack growth behavior of A250 and A300 materials using the different cyclic hardening characteristics (value n') in Eq. (7) to obtain an estimation of the respective behavior of the related positions in the HAZ in Fig. 3.

	Yield strength $\sigma_{0.2}$ (MPa)	Cyclic yield strength $\sigma_{c0.2}$ (MPa)	Strain hardening exponent n	Strength coefficient H (MPa)	Cyclic strain hardening exponent n'	Cyclic strength coefficient H' (MPa)
T3	375	445	0.120	694	0.042	576
A250	245	245	0.161	604	0.148	568
A300	135	185	0.242	594	0.211	674

Table 1: Cyclic and monotonic properties of T3, A250 and A300 materials.

CRACK GROWTH ANALYSIS

Crack closure under cyclic loads is influenced by the cyclic hardening mechanism at the crack tip. In [14-17] it was analytically and experimentally demonstrated that increased cyclic hardening contributes to increased crack closure and retards fatigue crack growth.

In Eq. (7), the cyclic hardening exponent n' was used to analyze the local fatigue crack growth behavior of the various positions in the HAZ (A250 and A300). In the analysis, the material properties included in parameter B (Eq. 10) for all materials have been taken from the reference, base metal, 2024 T3 alloy and are presented in Tab. 2. The material volume length r_c was fitted from the 2024 T3 data. In Fig. 6 the analytical results obtained using a numerical integration of Eq. (7) for T3 (base metal), A250 (mid-point HAZ gradient) and A300 (HAZ/TMAZ) materials are compared against experimental crack growth rates. Analytical and experimental crack growth rates agree well for the stress intensity factor range examined (12-25 MPa $m^{1/2}$), specifically for the position associated with A250, while for the case of A300 (HAZ/TMAZ interface) a small overestimation in predicted crack growth rates exists.

Cyclic hardening exponent n'	Parameter r_c (m)	Coffin-Manson exponent c	Coffin-Manson parameter ε_f'	critical stress intensity factor K_{cr} ($MPam^{1/2}$) [23]	Young's modulus E (GPa)	Poisson ratio ν
T3: 0.042 A250: 0.148 A300: 0.211	1.291×10^{-6}	-0.6	0.13	60	73.1	0.33

Table 2: Material parameters used in Eq. (7) for FCG analysis.

In Tab. 3 the average value of parameter r_c for the three materials T3, A250 and A300 is given. In Fig. 7 the analytical results are compared against the experimental crack growth rates using in the analysis the mean value of r_c in order to evaluate the sensitivity of the analysis on the fitting parameter. The differences in this case are negligible, which shows that analytical predictions are not influenced by the value of r_c.

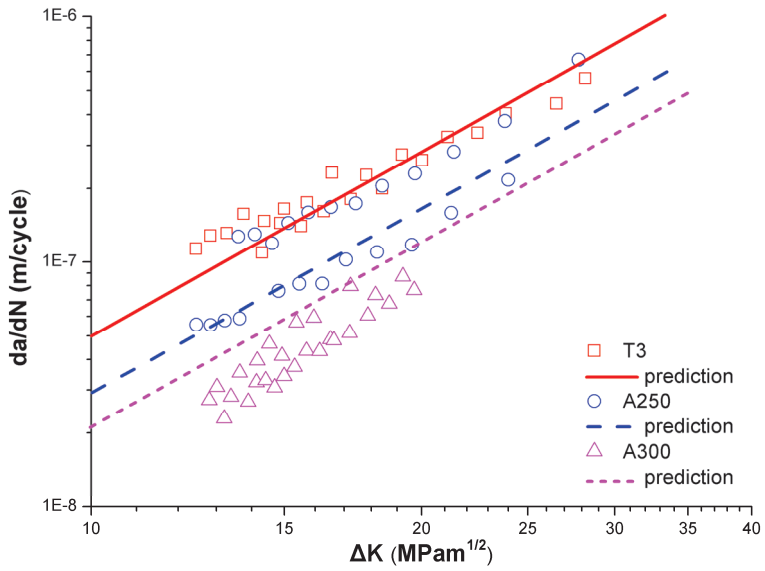

Figure 6: Experimental and computed fatigue crack growth rates vs. stress intensity factor range (dα/dN-ΔK) in T3, A250 and A300 materials. The analytical results were obtained for c=-0.6 and r_c=1.291x10^{-6} m.

	parameter r_c (m)	
T3	1.291x10^{-6}	*mean:* *1.329x10^{-6}*
A250	1.538x10^{-6}	
A300	1.158x10^{-6}	

Table 3: Average value of r_c length.

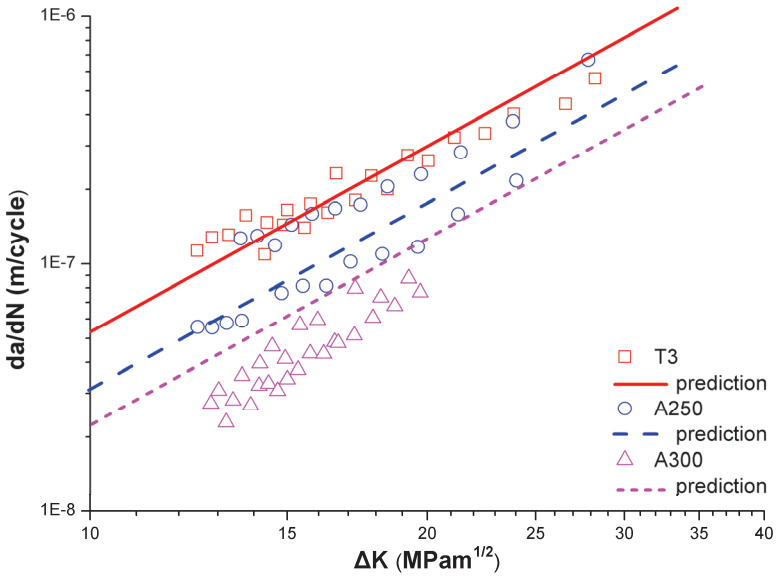

Figure 7: Experimental and computed fatigue crack growth rates vs. stress intensity factor range (dα/dN-ΔK) in T3, A250 and A300 materials evaluated for $r_{c,mean}$=1.329x10^{-6} m.

CONCLUSIONS

A model with the ability to perform fatigue crack growth analysis taking into account the local material behavior at specific locations in an aluminum 2024 T3 FSW Heat Affected Zone is proposed. To simulate the local material behavior in the HAZ without the effect of weld residual stresses, the reference 2024 T3 aluminum alloy was subjected to specific overaging conditions. The obtained overaged materials have very similar microstructural characteristics and mechanical properties to the HAZ material. The analytical results obtained with the model showed that it can satisfactory predict crack growth rates of the material with local HAZ characteristics.

ACKNOWLEDGMENTS

This research has been co-financed by the European Union (European SocialFund - ESF) and Greek national funds through the Operational Program"Education and Lifelong Learning" of the National Strategic Reference Framework (NSRF) - Research Funding Program: Heracleitus II. Investing in knowledge society through the European Social Fund.

REFERENCES

[1] Paris, P., Erdogan F., A Critical Analysis of Crack Propagation Laws. Journal of Fluids Engineering, 85 (4) (1963) 528-533. DOI:10.1115/1.3656900

[2] Rice, J.R., Mechanics of crack tip deformation and extension by fatigue. In fatigue Crack propagation. Special Technical Publication, American Society for Testing and Materials STP 415 247-309 (1967).

[3] Weertman, J., Rate of growth of fatigue cracks calculated from the theory of infinitesimal dislocations distributed on a plane. International Journal of Fracture Mechanics, 2 (2) (1666) 460-467. DOI 10.1007/BF00183823.

[4] McClintock, F.A., On the plasticity of the growth of fatigue cracks. Fracture of solids, 20 (1963) 65-102.

[5] Wu, S.-X., Mai Y.-W., Cotterell B., A model of fatigue crack growth based on Dugdale model and damage accumulation, International Journal of Fracture, 57 (3) (1992) 253-267. DOI: 10.1007/BF00035077.

[6] Shi, K.K., Cai L.X., Chen L., Wu S.C., Bao C., Prediction of fatigue crack growth based on low cycle fatigue properties. International Journal of Fatigue, 61 (0) (2014) 220-225. DOI:10.1016/j.ijfatigue.2013.11.007.

[7] Chen, L., Cai, L..X., Yao, D., A new method to predict fatigue crack growth rate of materials based on average cyclic plasticity strain damage accumulation. Chinese Journal of Aeronautics, 26 (1) (2013) 130-135. DOI:10.1016/j.cja.2012.12.013.

[8] Pandey, K.N., Chand, S., An energy based fatigue crack growth model, International Journal of Fatigue, 25 (8) (2003) 771-778. DOI:10.1016/S0142-1123(03)00049-5.

[9] Kermanidis, A.T., Pantelakis, S.G., Fatigue crack growth analysis of 2024 T3 aluminium specimens under aircraft service spectra. Fatigue & Fracture of Engineering Materials & Structures, 24 (10) (2001) 699-710. DOI: 10.1046/j.1460-2695.2001.00435.x.

[10] Reifsnider, K., Kahl, M., Effect of local yield strength gradients on fatigue crack propagation, International Journal of Mechanical Sciences, 16 (2) (1974) 105-119. DOI:10.1016/0020-7403(74)90080-0.

[11] Scialpi, A., de Filippis, L.A.C., Cavaliere, P., Influence of shoulder geometry on microstructure and mechanical properties of friction stir welded 6082 aluminium alloy, Mater Design, 28 (2007) 1124–1129. DOI:10.1016/j.matdes.2006.01.031.

[12] Cavaliere, P., Nobile, R., Panella, F.W., Squillace, A., Mechanical and microstructural behavior of 2024-7075 aluminium alloy sheets joined by friction stir welding, Int J Mach Tool Manufac, 46 (2006) 588–594. DOI:10.1016/j.ijmachtools.2005.07.010.

[13] Ceschini, L., Boromei, I., Minak, G., Morri, A., Tarterini, F., Effect of friction stir welding on microstructure, tensile and fatigue properties of the AA7005/10 vol.%Al2O3p composite, Compos Sci Technol, 67 (2007) 605–615. DOI:10.1016/j.compscitech.2006.07.029.

[14] Tzamtzis, A., Kermanidis, A. T., Improvement of fatigue crack growth resistance by controlled overaging in 2024-T3 aluminium alloy, Fat. &. Fract. Eng . Mat and Struct., 37(7) (2014) 751-763. DOI: 10.1111/ffe.12163.

[15] Budiansky, B., Hutchinson, J.W., Analysis of Closure in Fatigue Crack Growth. Journal of Applied Mechanics, 45(2)

(1978) 267-276.
[16] Pommier, S., Plane strain crack closure and cyclic hardening. Engineering Fracture Mechanics, 69 (1) (2002) 25-44. DOI:10.1016/S0013-7944(01)00061-3.
[17] Chang, T., Guo, W., Effects of strain hardening and stress state on fatigue crack closure. International Journal of Fatigue, 21 (9) (1999) 881-888. DOI:10.1016/S0142-1123(99)00085-7.
[18] Morrow, J., Cyclic plastic strain energy and fatigue of metals. Internal Friction, Damping and Cyclic Plasticity, ASTM STP, 378 (1965) 45-87. DOI: 10.1520/STP378-EB.
[19] Sih, G.C., Methods of analysis and solutions of crack problems. Springer, 1 (1973). DOI:10.1007/978-94-017-2260-5.
[20] Sih, G.C., Some basic problems in fracture mechanics and new concepts. Engineering Fracture Mechanics, 5(2) (1973) 365-377. DOI:10.1016/0013-7944(73)90027-1.
[21] Manson, S.S., Fatigue: A complex subject-Some simple approximations. Experimental Mechanics, 5 (4) (1965) 193-226. DOI:10.1007/BF02321056.
[22] Tavernelli, J.F., Coffin, J.L.F., Experimental Support for Generalized Equation Predicting Low Cycle Fatigue, Journal of Fluids Engineering, 84 (4) (1962) 533-537. DOI:10.1115/1.3658701.
[23] Kermanidis, A.T., Tzamtzis, A., Prediction of fatigue crack propagation in aluminum alloy with local yield strength gradient at the crack path, 14th International Congress on Mesomechanics, Budapest, Hungary (2012).